



1 **Stratospheric aerosol formed from the boiling sea induced by**  
2 **the 2022 Hunga Ha’apai volcanic eruption**

3  
4 Bengt G. Martinsson, Johan Friberg, Moa K. Sporre

5 Department of Physics, Lund University, Lund, Sweden

6 *Correspondence to:* Bengt G. Martinsson (bengt.martinsson@fysik.lu.se)

7 **Abstract.** Hot volcanoclastic density currents entering the sea from the Hunga Tonga eruption the 15 January  
8 2022 (HT-22) induced vigorous volcano – sea interaction. Here we study the stratospheric aerosol and water  
9 vapor resulting from the eruption using satellite-based instruments: the CALIOP lidar and the Microwave Limb  
10 Sounder (MLS). We investigate the stratospheric relative humidity following the record-breaking water vapor  
11 injections from the HT-22 eruption, and the particle size of the aerosol. The HT-22 eruption injected its effluents  
12 into the deep Brewer-Dobson (BD) branch causing several years of stratospheric perturbation. The long  
13 duration, and aerosol concentration among the highest, makes the HT-22 eruption the strongest stratospheric  
14 aerosol event since the 1991 Mt. Pinatubo eruption despite a modest SO<sub>2</sub> injection explaining only ~30% of the  
15 AOD from the HT-22 eruption according to our estimates. The stratospheric AOD level was established after 2  
16 weeks, or possibly even earlier, which is a short time compared with the usual 2 – 3 months required to reach  
17 the maximum AOD following volcanic eruptions. We discuss the sources of the aerosol from the HT-22 eruption  
18 in relation to the low emission of SO<sub>2</sub>, its e-folding time and volcanological observations of strong interactions  
19 with the sea containing not only water but also high concentrations of dissolved substances.

20 **1 Introduction**

21 The stratospheric background conditions are frequently offset by injections of copious amounts of aerosol and  
22 gases from explosive volcanic eruptions (Kremser et al., 2016) and intense wildfires forming  
23 pyrocumulonimbus clouds (Fromm et al., 2010). These events cause variable stratospheric impact with  
24 durations of months to several years (Friberg et al., 2018), which are important to account for in climate models  
25 (Schmidt et al., 2018).

26 The Hunga Tonga – Hunga Ha’apai volcano erupted on 15 January 2022, with a volumetric flow rate an order of  
27 magnitude higher than that of the 1991 Mt Pinatubo eruption. The eruptions formed an umbrella cloud at 31 km  
28 and a second cloud at 17 km altitude (Gupta et al., 2022). Further, a record-breaking overshooting plume  
29 reached above 50 km (Carr et al., 2022, Proud et al., 2022, Taha et al., 2022). The volcanic explosivity index  
30 (VEI) was estimated to be 6, based on seismological observations (Poli and Shapiro, 2022). Despite the high  
31 VEI, ash could not be detected in the ice-rich stratospheric clouds from the HT-22 eruption (Gupta et al., 2022),  
32 and the UV aerosol index (UVAI) indicates low ash content (Carn et al., 2022). This is further supported by  
33 CALIOP (Cloud-Aerosol LIdar with Orthogonal Polarization) measurements finding very low depolarization  
34 ratios indicating dominance of spherical particles uncharacteristic of ash (Legras et al., 2022). Additionally, the  
35 volcanic layers in the stratosphere contained very low SO<sub>2</sub> amounts for such a strong eruption (Carn et al.,  
36 2022).



37 Widespread damage to the seafloor with runouts exceeding 100 km was caused by volcanoclastic density  
38 currents, suggesting a collapsing eruption column entering the sea (Seabrook et al., 2023; Clare et al., 2023).  
39 Such a sequence of events where hot volcanoclastic density currents form induces intense boiling of the sea over  
40 vast areas, supplying hot water vapor forming a plume that is buoyant at the base and accelerates as it rises. A  
41 relatively small eruption can in this way form umbrella clouds the size and altitude of the HT-22 eruption,  
42 whereas entrainment of vapor from cold water does not (Mastin et al., 2024).

43 The stratospheric background aerosol contains mainly sulfurous and carbonaceous components with some  
44 extraterrestrial and tropospheric components (Murphy et al., 2007, Kremser et al., 2016, Martinsson et al.,  
45 2019). Volcanic aerosol in the stratosphere normally contains large amounts of sulfuric acid formed from sulfur  
46 dioxide (SO<sub>2</sub>), water, carbonaceous material and ash (Martinsson et al., 2009; Andersson et al., 2013; Friberg et  
47 al., 2014). Wildfires produce an aerosol initially dominated by organic and black carbon (Garofalo et al., 2019),  
48 where the former component is rapidly removed by photolysis (half-life 10 days) in the stratosphere (Martinsson  
49 et al., 2022; Friberg et al., 2023).

50 The volcanic and wildfire events also affect particle size distribution. During a long period with conditions close  
51 to the background, spanning 1998 to 2004, the particle volume mode was 0.2 – 0.3 μm in diameter, whereas  
52 approximately 1 μm in 1992 – 1993 after the Mt. Pinatubo eruption (Bauman et al., 2003; Wilson et al., 2008).  
53 Measurements the second week after the 2017 Canadian wildfire showed particle diameter of 0.6 – 0.7 μm  
54 (Haarig et al., 2018; Hu et al., 2019).

55 In this work we investigate the stratospheric aerosol resulting from the HT-22 eruption in relation to the  
56 volcanological sequence of events during the eruption. We also investigate the interaction of the aerosol with the  
57 large amounts of water vapor injected into the stratosphere. The global stratospheric aerosol optical depth  
58 (AOD) is studied 1.5 years after the eruption, until the decommission of the NASA satellite CALIPSO (Cloud-  
59 Aerosol Lidar and Infrared Pathfinder Satellite Observation) and its lidar sensor CALIOP. Our incrementally  
60 developed evaluation software (Andersson et al., 2015; Friberg et al., 2018; Martinsson et al., 2022) based on  
61 methodology presented in Vernier et al., (2011) was applied on CALIOP level 1B data. In contrast to limb-  
62 oriented methodology, the nadir-oriented CALIOP provides viable results in dense aerosol layers from strong  
63 volcanic eruptions and wildfires after correction for attenuation (Martinsson et al., 2022). We also use the  
64 satellite Aura sensor MLS for measurements of water vapor and temperature. We find that the SO<sub>2</sub> emissions  
65 from the HT-22 eruption cannot alone explain the high AOD level, nor can ash particles. We also find that the  
66 aerosol went deep into the stratosphere and that the one-year AOD perturbation due to the HT-22 eruption is the  
67 largest since that of Mt. Pinatubo in 1991.

## 68 **2 Methods**

69 Two satellite-based instruments were used to investigate the stratosphere following the HT-22 eruption. Aerosol  
70 measurements were based on the CALIOP lidar aboard CALIPSO, whereas water vapor concentrations and  
71 atmospheric temperature were obtained from MLS aboard Aura.

### 72 **2.1 CALIOP measurements**



73 CALIPSO orbits the globe 14 – 15 times per day between 82° S and 82° N. The vertical resolutions of CALIOP  
74 are 30, 60, 180 and 300 m in the altitude ranges <8.2, 8.2 – 20.2, 20.2 – 30.1 and 30.1 – 40 km, respectively  
75 (Winker et al., 2007, 2010). The average global stratospheric AOD from the tropopause (obtained from the  
76 MERRA-2 reanalysis (Modern-Era Retrospective analysis for Research and Applications)) to 35 km altitude in  
77 the stratosphere was computed from version 4-51 of CALIOP level 1B at the wavelength 532 nm using night-  
78 time measurements. The stratospheric AOD was computed in three layers: the lowermost stratosphere (LMS,  
79 tropopause to 380 K isentrope), the shallow BD branch (380 – 470 K isentropes) and deep BD branch (470 K  
80 isentrope – 35 km altitude), where potential temperatures were obtained from MERRA-2 pressures and  
81 temperatures. The effective lidar ratio was estimated based on single, intense volcanic layers day 1 – 28 after the  
82 eruption. From initial high values (70 sr) the lidar ratio declined to  $47.5 \pm 10.2$  sr. This is close to the commonly  
83 used CALIOP effective lidar ratio of 50 sr, which we therefore applied in this study. The attenuated backscatter  
84 CALIOP data were corrected by methods described in Martinsson et al. (2022). Based on measured parallel and  
85 perpendicularly polarized scattering, the volume depolarization was obtained and converted to particle  
86 depolarization ratios with methods described in Martinsson et al. (2022). Data were missing for a week from a  
87 few days after the eruption, and a long gap appeared from 21 October to 7 December 2022. Several minor gaps  
88 appeared during the first half-year of 2023 the last data produced by CALIOP. The CALIOP data evaluation  
89 methodology we use was originally developed by Vernier et al. (2011) and has been further developed in three  
90 steps (Andersson et al., 2015; Friberg et al., 2018; Martinsson et al., 2022), where more details on the  
91 methodology can be found.

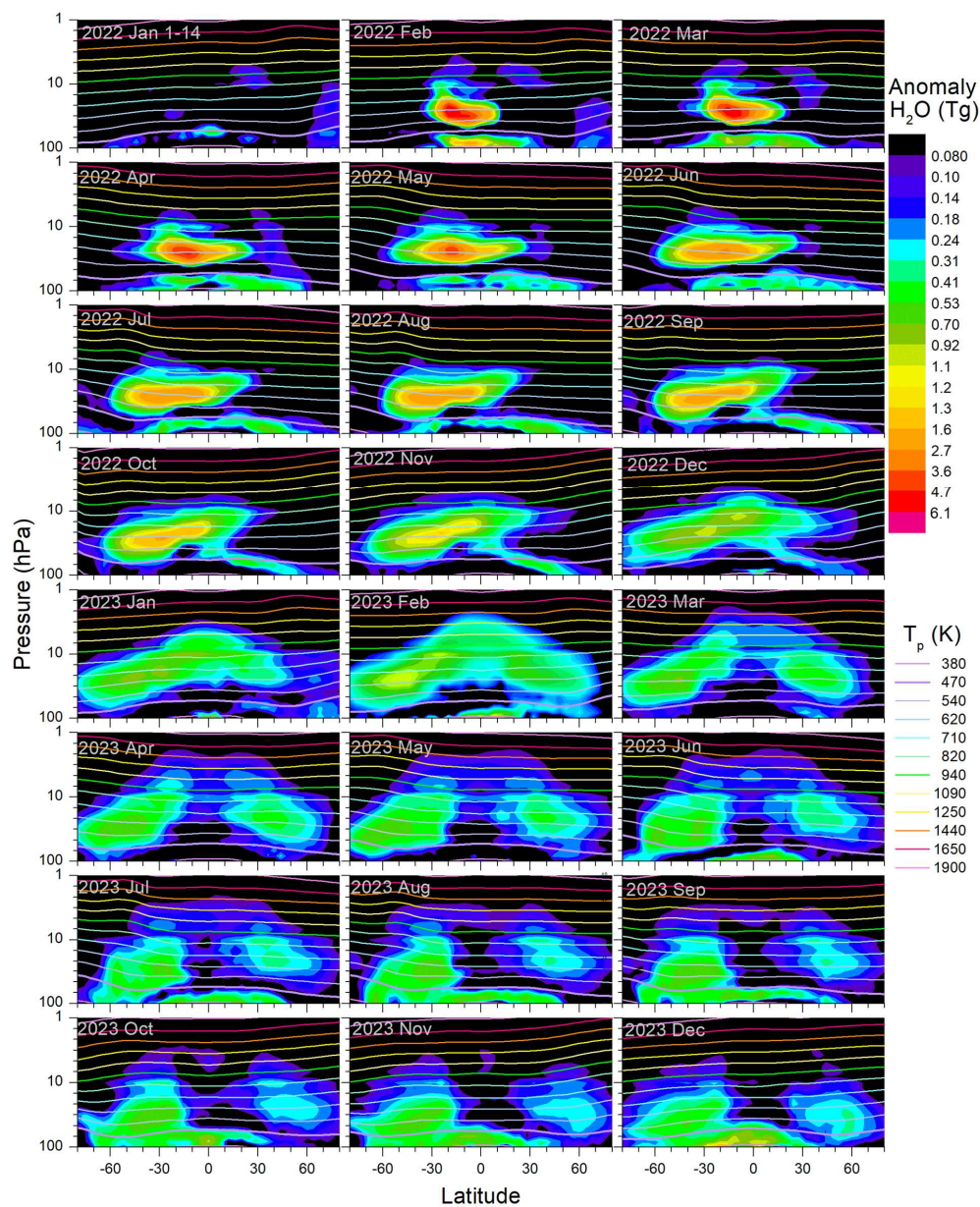
## 92 **2.2 MLS measurements**

93 Water vapor concentrations were obtained in the 100 – 1 hPa range in 12 levels per decade from the MLS,  
94 version 5.0-1.0a, level 2 (Waters et al., 2006). The vertical resolution is 1.3 – 3.6 km (Lambert et al., 2020;  
95 Livesey et al., 2020). Data were screened based on error parameters supplied with the data, rendering a large  
96 fraction of the volcanic data invalid the first two weeks after the eruption. From the beginning of February 2022,  
97 when our evaluation starts, erroneous data became scarce.

98 Stratospheric temperatures in the pressure range 100 – 1 hPa were obtained from the MLS, which were used  
99 primarily to compute relative humidity and potential temperature. The latter allows analysis of transport in  
100 relation to isentropic surfaces. The potential temperatures were also used as a common ground in comparisons  
101 between MLS and CALIOP, where the native vertical scale of the former is atmospheric pressure and for the  
102 latter geometric altitude.

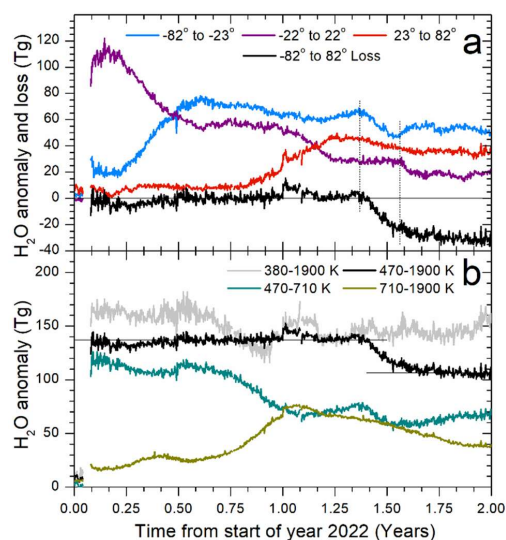
## 103 **3 Results**

104 This work focuses on the stratospheric aerosol resulting from the HT-22 eruption. The altitude and latitude  
105 distributions will be presented here together with the evolution of the stratospheric aerosol extinction  
106 coefficients and AOD. However, we start by presenting stratospheric water vapor data from the HT-22 eruption  
107 to highlight the contrasting evolution of the two volcanic components. Water vapor data are also used for  
108 computations on relative humidity and vertical air motions presented in the Discussion section.



109

110 **Figure 1.** Monthly averaged H<sub>2</sub>O mass anomaly (Tg) against latitude and altitude with pixel size  $(2.3 \pm 0.14) \times$   
111  $10^{16} \text{ m}^3 \text{ times } \cos(\Theta)$ , where  $\Theta$  is the latitude. Note that “2022 Jan 1 – 14” covers only the pre-eruption period 1  
112 – 14 January. Overlain isentropes in the range 380 – 1900 K are shown, where  $T_p$  is the potential temperature.  
113 Note that the 380 K isentrope reaches below 100 hPa only in the tropics and that the 1900 K isentrope partly is  
114 found at pressures below 1 hPa. Vertical scale minor ticks: 1.5, 2.2, 3.2, 4.6, 6.8 and ten times these values.



115

116 **Figure 2.** Evolution of water vapor ( $\text{H}_2\text{O}$ ) anomaly following the January 15, 2022, Hunga Tonga eruption. **a)**  
 117  $\text{H}_2\text{O}$  anomaly in three latitude intervals and loss of  $\text{H}_2\text{O}$  in a 4th latitude interval, all in the  $470 < T_p < 1900$  K  
 118 range (the deep BD branch). Vertical lines mark the main region of  $\text{H}_2\text{O}$  loss of the deep BD branch. **b)**  $\text{H}_2\text{O}$   
 119 anomaly in the latitude interval  $-82$  to  $82^\circ$  in various potential temperature intervals ( $T_p$ ). Horizontal lines show  
 120 the average  $\text{H}_2\text{O}$  anomaly from end of January 2022 to mid-May 2023 ( $136.9 \pm 0.2$  (standard error) Tg) and from  
 121 the beginning of October to the end of December 2023 ( $106.1 \pm 0.3$  Tg).

### 122 3.1 Water vapor

123 It has widely been reported about the record-breaking amounts of water vapor reaching the stratosphere  
 124 following the HT-22 eruption (Millán et al., 2022; Schoeberl et al., 2022; Xu et al., 2022; Zhu et al., 2022;  
 125 Nedoluha et al., 2024). Here we present the distribution related to isentropic surfaces in contrast to previous  
 126 authors, in particular the fate of water that reaches the deep branch of the BD circulation, i.e., above the  
 127 potential temperature ( $T_p$ ) 470 K (Fueglistaler et al., 2009). Fig. 1 shows monthly mean water vapor mass  
 128 anomalies for years 2022 and 2023, where the masses of year 2021 were subtracted, the exception being January  
 129 2022 where only the days prior to the eruption are shown (January 1 – 14). The first two weeks after the  
 130 eruption the MLS water vapor data from volcanic effluents frequently were erratic, probably due to high  
 131 concentrations, and are not shown.

132 In February 2022 two layers appear, one minor in the shallow BD branch and the main layer in the deep BD  
 133 branch, consistent with the reported eruption chronology (Gupta et al., 2022). The lower water vapor layer is  
 134 spread rapidly latitudinally before it is transported below the lower atmospheric pressure limit used here (100  
 135 hPa).

136 The first months after the eruption the water of the upper layer remains in the tropics, before a fraction clearly  
 137 visible in May 2022 is transported to the Southern extratropics (Figs. 1 and 2a). Towards the end of 2022



138 transport to the Northern extratropics starts, and in February 2023 the water from the HT-22 eruption covers  
139 most of the globe. Later that year most of the water is found in the extratropics, whereas the water-rich air in the  
140 tropics is replaced in the BD circulation by younger tropospheric air that is unaffected by the HT-22 eruption  
141 (Figs. 1 and 2a). At the same time the water in the Southern extratropics of the deep BD branch approaches and  
142 clearly passes the 470 K isentrope in May 2023 (Fig. 1 and 2a), consistent with the extratropical downward  
143 motion of air.

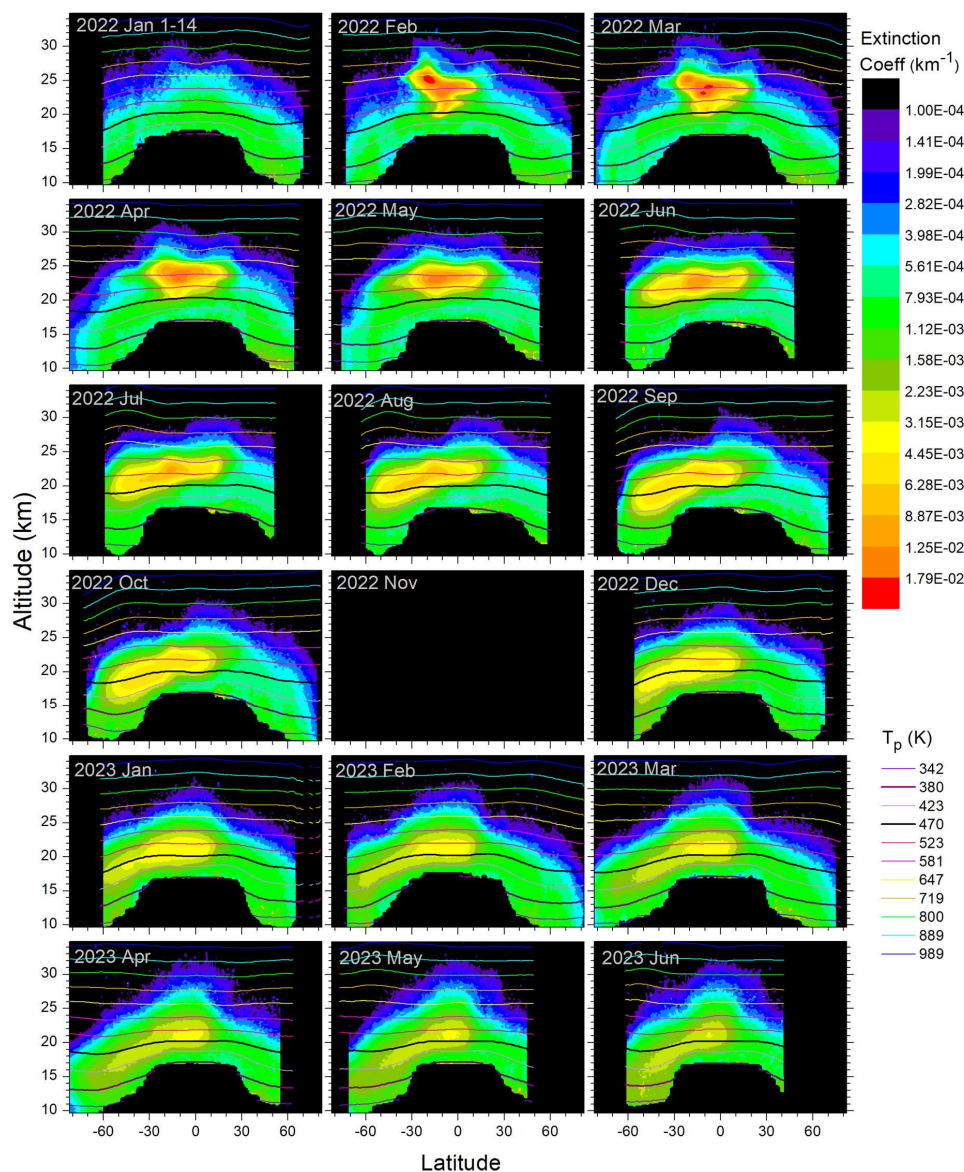
144 The total amount of water vapor from the HT-22 eruption in the stratosphere at  $T_p > 380$  K in the tropics and  
145 100 hPa atmospheric pressure elsewhere, is 160 Tg. The mass in the deep BD branch, which is a part of the  
146 previously mentioned layer, is 138 Tg. After  $\frac{3}{4}$  of a year these categories reach the same level (Fig. 2b),  
147 implying that the lower water layer (injected below the deep BD branch) is transported down below the lower  
148 limit in altitude (atmospheric pressure 100 hPa) of the data used here. The water vapor displays considerable  
149 vertical transport in the deep BD branch. Dividing that branch into two  $T_p$  intervals (Fig. 2b) reveals a clear rise  
150 in the amount of water in the upper interval in the last quarter of the year 2022. A small fraction of the water  
151 vapor reached high altitudes in the tropics during the year 2023 (Fig. 1), and some even reached altitudes above  
152 1 hPa atmospheric pressure ( $\sim 48$  km), i.e. the region of the stratopause (supplementary Fig. S1).

153 The water anomaly remained constant in the deep BD branch with only minor fluctuations from February 2022  
154 to May 2023 (Fig. 2b), whereafter the anomaly is reduced by 23% due to transport to the shallow BD branch, a  
155 level that remains until the end of 2023.

### 156 3.2 Aerosol

157 The evolution of the stratospheric AOD following the HT-22 eruption has been reported by several authors using  
158 limb-viewing measurements (Bourassa et al., 2022; Sellitto et al., 2022; Taha et al., 2022) that suffer from event  
159 termination (“saturation”) during the first months after strong volcanic or wildfire events (Fromm et al., 2014;  
160 Chen et al., 2018; DeLand et al., 2019; Martinsson et al., 2022), and problems to measure the lower parts of the  
161 stratosphere (Taha, 2020). Here we present results based on a nadir-viewing lidar technique (CALIOP) that is  
162 better suited for measurements in dense aerosol layers because they do not suffer from saturation effects, and  
163 attenuation of the lidar signal can be corrected for (Martinsson et al., 2022).

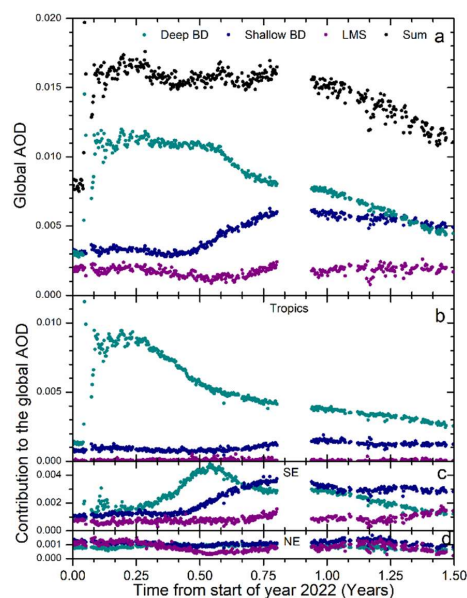
164 Just as for water vapor, we present monthly mean values of the aerosol distribution with overlaid isentropic  
165 surfaces (Fig. 3). January 2022 aerosol data show conditions prior to the eruption. Initially (February – June  
166 2022) almost all the HT-22 aerosol is found in the deep BD branch ( $T_p > 470$  K). We identify downward motion  
167 of the aerosol centroid in the tropics, the most intense part shifting from isentrope 581 to 523 K from March to  
168 September 2022, despite the upward motion of air in the tropics as part of the BD circulation. This is caused by  
169 gravitational settling, and the aerosol that reaches the Southern extratropics loses altitude even faster, aided by  
170 downward air motion in the extratropics, leading to an increasing fraction of the aerosol in the shallow BD  
171 branch from July 2022. The aerosol continues downwards, reaching the LMS (below 380 K) in December 2022  
172 on its way out of the stratosphere.



173

174 **Figure 3.** Monthly average extinction coefficients dependent on latitude and altitude with overlaid potential  
175 temperature levels. Note that “2022 Jan 1 – 14” covers only the pre-eruption period 1 – 14 January.

176 Substantial amounts of aerosol entered the stratosphere because of the HT-22 eruption. The global average AOD  
177 reached 0.016 (Fig. 4a), which is among the highest stratospheric aerosol loads since the 1991 Mt. Pinatubo  
178 eruption. Already by the end of January, half a month after the eruption, the AOD level that remained for almost  
179 a year was reached. After that we see a decline where approximately half of the aerosol from the HT-22 eruption  
180 is removed during the first half-year of 2023. Almost the entire aerosol amount from HT-22 was found in the



181

182 **Figure 4. a)** Global average AOD of the stratosphere from the tropopause to 35 km altitude and -82 to 82° in  
 183 latitude (Sum) with the sub layers: the tropopause to 380 K potential temperature ( $T_p$ ) (LMS), 380 – 470 K  $T_p$   
 184 (shallow Brewer-Dobson (BD) branch) and  $T_p$  470 K to 35 km altitude (deep BD). Latitude distributions of  
 185 AOD **b)** tropics (-22 to 22°), **c)** Southern extratropics (SE) (-82 to -23°) and **d)** Northern extratropics (NE) (23  
 186 to 82°). The AODs are related to the global scale, i.e. the sum of SE, tropics and NE graphs is the global AOD.

187 deep BD branch the first months after the eruption (Fig. 4a), in the tropics (Fig. 4b). We see transport to the  
 188 Southern extratropics starting in April 2022 in the deep BD followed by downward motion to the shallow BD  
 189 branch starting in June 2022 (Fig. 4c). Only a small fraction of the aerosol reached the Northern extratropics  
 190 (Fig. 4d), in contrast to the transport of water vapor (Fig. 2a) that took place at a higher altitude (Fig.1).

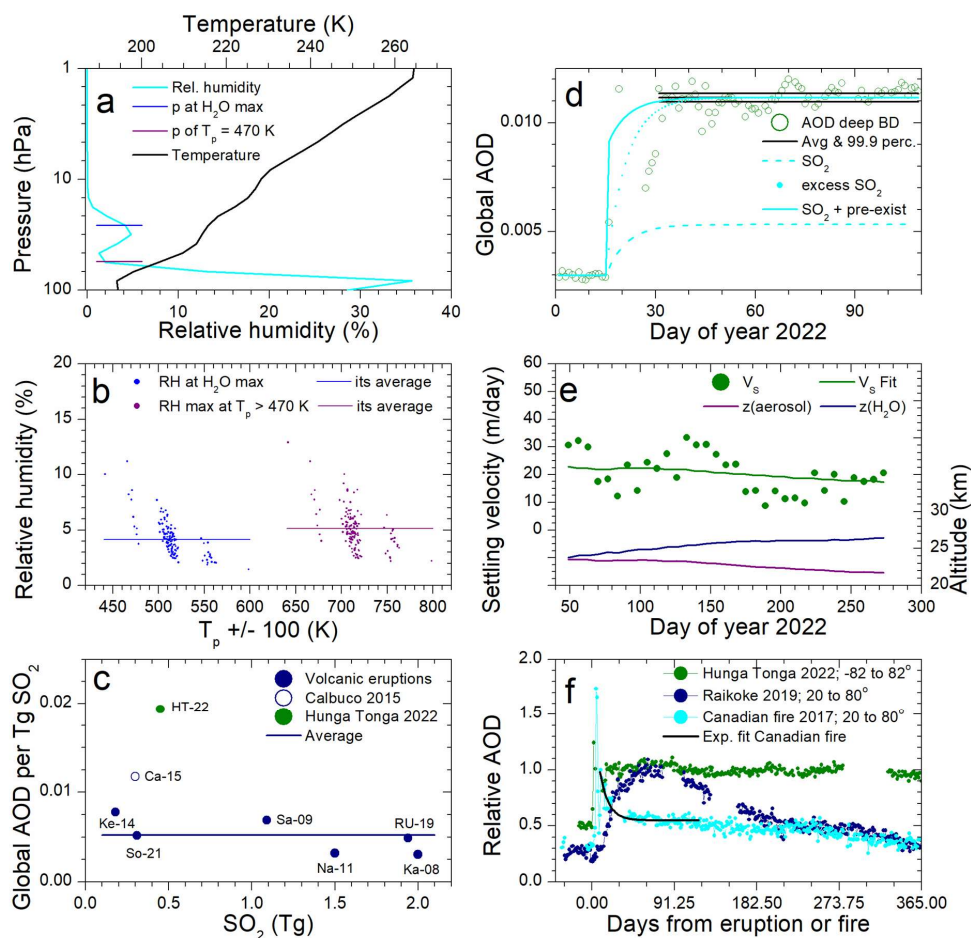
#### 191 4 Discussion

192 SO<sub>2</sub> emissions from HT-22 eruptions took place over a period from 19 December 2021 to 15 January 2022  
 193 (Carn 2022). Most of these eruptions reached 15 – 18 km in altitude, whereas the main eruption’s umbrella  
 194 cloud on 15 January 2022 reached 31 km with an overshooting plume reaching 55 – 58 km (Gupta et al., 2022).  
 195 Based on several methods the total SO<sub>2</sub> emissions during this period is estimated to 0.6 – 0.7 Tg, and that of the  
 196 main umbrella cloud, reaching deep into the stratosphere, contained 0.4 – 0.5 Tg SO<sub>2</sub> (Carn et al., 2022).  
 197 Altitude-resolved SO<sub>2</sub> measurements from MLS find a similar SO<sub>2</sub> amount deep into the stratosphere (Millán  
 198 2022). Compared with the SO<sub>2</sub> emissions, the stratospheric AOD generated by the HT-22 eruption is  
 199 unexpectedly high. Here we will discuss reasons for this seeming discrepancy, and we start by examining water  
 200 uptake as an explanation.



201 The temperature is rising with altitude in the stratosphere, making the air very dry after passing the tropical cold  
202 point tropopause. The amount of water vapor injected by the HT-22 eruption is unprecedented in the modern  
203 satellite era (Zhu et al., 2022). It has been suggested that hygroscopic growth could be an important process that  
204 affects the aerosol particle size and light scattering (Legras et al., 2022; Sellitto et al., 2022). Here we investigate  
205 the relative humidity by examining the five highest daily water vapor concentrations measured by the MLS  
206 during February 2022 (140 MLS profiles), when the volcanic effluents were concentrated to a relatively small  
207 volume. Based on MLS water vapor and temperature measurements the relative humidity was computed, where  
208 the saturation water vapor pressures were obtained from Murphy and Koop (2005). Fig. 5a shows the average  
209 relative humidity of the profiles (140) from February 2022. At the lowest altitudes, close to 100 hPa, the relative  
210 humidity reaches 35% because of the low temperature (Fig. 5a, upper scale), and, to a smaller degree, the lower  
211 volcanic layer (Fig. 1, February 2022). At higher altitude, the relative humidity rapidly declines as the  
212 temperature increases, becoming close to zero at altitudes above 10 hPa. However, a peak appears at 30 hPa  
213 caused by the main volcanic layer (above 470 K potential temperature) containing most of the stratospheric  
214 water vapor from the HT-22 eruption (Fig. 2b). In the following discussion we concentrate on that layer. The  
215 average positions of the 470 K isentrope and the peak water vapor concentration are shown in Fig. 5a, where the  
216 shift of the maximum relative humidity from the peak water vapor concentration is caused by the temperature  
217 gradient. The relative humidity at the peak water vapor concentration as well as the maximum relative humidity  
218 of all the 140 mentioned measurements are shown in Fig. 5b (note the shift of  $\pm 100$  K in potential temperature  
219 to separate the two categories). The measurements of each of the two categories appear in groups depending on  
220 the altitude (or pressure level) of the water vapor layer. The maximum relative humidity above the 470 K  
221 isentrope is 13%, and that of the peak water vapor is 11%, whereas the averages are 5.1 and 4.2%. Such low  
222 relative humidities causes no or modest hygroscopic growth (Winkler, 1973) that affects particle size or light  
223 scattering only to a small degree.

224 Several authors regard the aerosol from the HT-22 eruption as a sulfate aerosol (Khaykin et al., 2022; Legras et  
225 al., 2022; Sellitto et al., 2022; Taha et al., 2022; Zhu et al., 2022; Bernath et al., 2023; Duchamp et al., 2023;  
226 Kahn et al., 2024; Sellitto et al., 2024), although with questions on the relatively small amount of SO<sub>2</sub> emitted in  
227 relation to the AOD level (Carn et al., 2022). Here we will investigate this relation in more detail by forming the  
228 ratio of the maximum global stratospheric AOD rise above the pre-eruption AOD to the amount of SO<sub>2</sub> emitted  
229 by eight recent volcanic eruptions (Table 1 and Fig. 5c). This ratio is approximately 0.005 Tg<sup>-1</sup> for most of the  
230 eruptions, whereas the Calbuco (Ca-15) and HT-22 deviate by having higher AOD per SO<sub>2</sub> mass emitted. Most  
231 of these volcanic eruptions showed depolarization ratio less than 0.05 (Hoffmann et al., 2010; O'Neill et al.,  
232 2012; Zhuang & Yi 2016; Voudouri et al., 2023) typical of aerosol dominated by spherical sulfuric acid  
233 particles. Volcanic ash settles rapidly by gravitation, but a fraction can remain for months in the stratosphere  
234 (Andersson et al., 2013). Vernier et al. (2016) found that this can affect stratospheric AOD, detecting elevated  
235 depolarization ratio (0.05) a month after the Kelut eruption (Ke-14). The depolarization ratio of the aerosol from  
236 the Ca-15 eruption was much higher (0.18) a month after the eruption (Klekociuk et al., 2020) thus indicating a  
237 strong influence from ash on the AOD that likely explains the strong deviation in AOD-to-SO<sub>2</sub> ratio from the  
238 other eruptions. Ca-15 was therefore not included in the average AOD-to-SO<sub>2</sub> ratio calculated here. The HT-22  
239 eruption has the highest AOD-to-SO<sub>2</sub> ratio but low depolarization ratio (supplementary Fig. S2), thus high ash  
240 concentration is not a valid explanation (Gupta et al., 2022; Carn et al., 2022; Legras et al., 2022).



241

242 **Figure 5.** Stratospheric characteristics after the HT-22 eruption. **a)** Average relative humidity (RH) and  
 243 temperature of the five daily H<sub>2</sub>O profiles with the highest concentration during February 2022. **b)** RH at the  
 244 maximum H<sub>2</sub>O concentration and maximum RH at potential temperatures > 470 K of all the profiles mentioned  
 245 in (a) with average RH of 4.2 and 5.1%, respectively. The potential temperature (T<sub>p</sub>) was shifted ± 100 K to  
 246 separate the two groups of data. **c)** Global AOD per Tg SO<sub>2</sub> emitted by recent volcanic eruptions related to SO<sub>2</sub>,  
 247 the average being 0.0052 global AOD per Tg SO<sub>2</sub> (see Table 1). **d)** AOD in the upper BD branch with 99.9  
 248 percentile of the average marked and reported SO<sub>2</sub> of 0.45 Tg (Carn et al., 2022) converted to AOD according to  
 249 (c) (broken line), and the dotted line tests the evolution using an excess of 1.1 Tg SO<sub>2</sub> to reach the measured  
 250 AOD. The full cyan line displays the SO<sub>2</sub> AOD (broken line) added by an assumed AOD from pre-existing  
 251 aerosol from the eruption to reach the measured AOD. **e)** Aerosol gravitational settling velocity (V<sub>s</sub>) and fit  
 252 (equivalent aerodynamic diameter 1.1 μm) and average altitudes (z; right scale) of the HT-22 aerosol and water  
 253 vapor at latitudes -14 to -6°. **f)** Normalized stratospheric AOD evolution during one year for one wildfire event  
 254 (Martinsson et al., 2022) and two volcanic eruptions.



255 **Table 1.** Recent volcanic eruptions with SO<sub>2</sub> emissions, global stratospheric optical depths (AOD) and literature  
256 references.

Date	Eruption	Short name	SO <sub>2</sub> (Tg)	SO <sub>2</sub> references	Global AOD <sup>a</sup>	Depolarization Ratio references
2008-08-07	Kasatochi	Ka-08	2	Yang et al., 2010	0.0061	Hoffmann et al., 2010
2009-06-12	Sarychev	Sa-09	1.09	Sandvik et al., 2021	0.0075	O'Neill et al., 2012
2011-06-12	Nabro	Na-11	1.5	Clarisse et al., 2012	0.0048	Zhuang & Yi 2016
2014-02-14	Kelut	Ke-14	0.18	Li et al., 2017	0.0014	Vernier et al., 2016
2015-04-23	Calbuco	Ca-15	0.3	Pardini et al., 2018	0.0035	Klekociuk et al., 2020
2019-06-22	Raikoke		1.5			
2019-06-26	Ulawun	RU-19	0.14	Kloss et al., 2021	0.0095	Voudouri et al., 2023
2019-08-03	Ulawun		0.3			
2021-04-10	Soufriere	So-21	0.31	Taylor et al., 2023	0.0016	<sup>b</sup> Lidar browse images
2022-01-15	Hunga Tonga	HT-22	0.45	Carn et al., 2022	0.0087	This work

257 <sup>a</sup>) Global stratospheric AOD maximum increase due to the eruptions. References: Friberg et al., 2018 and this  
258 work (2019 – 2023)

259 <sup>b</sup>) Lidar Level 1 Browse Images - 2021-04-26 09:42:19Z - Section 1 ([https://www-](https://www-calipso.larc.nasa.gov/products/lidar/browse_images/std_v451_index.php)  
260 [calipso.larc.nasa.gov/products/lidar/browse\\_images/std\\_v451\\_index.php](https://www-calipso.larc.nasa.gov/products/lidar/browse_images/std_v451_index.php))

261 We adopt the central estimate of Carn et al. (2022), i.e., 0.45 Tg SO<sub>2</sub> with an e-folding time of ~6 days. The e-  
262 folding time is unusually short for stratospheric conditions, probably due to elevated water vapor concentrations  
263 (Carn et al., 2022). Fig. 5d shows the AOD, with double-sided 99.9% confidence interval of the mean in the  
264 deep BD branch, where all the aerosol from the HT-22 eruption was injected (Fig. 4a). Using the AOD-to-SO<sub>2</sub>  
265 ratio based on six volcanic eruptions (Fig. 5c) to estimate the AOD based on the SO<sub>2</sub> emissions, we end up with  
266 far too low AOD (Fig. 5d, broken line). To investigate the timing, we added 1.1 Tg excess SO<sub>2</sub> to reach the  
267 measured AOD while preserving the measured e-folding time (dotted line). The excess SO<sub>2</sub> reaches into the  
268 99.9% confidence interval of the average AOD after approximately 50% longer time from the eruption  
269 compared to the time required for CALIOP to record a stable AOD. It is thus unlikely that the aerosol from the  
270 HT-22 eruption was formed from SO<sub>2</sub> conversion alone, mainly because of the low SO<sub>2</sub> emissions, but also  
271 because of the timing. Other material must have been present already the first days after the eruption. Making  
272 use of the AOD-to-SO<sub>2</sub> ratio from Fig. 5c, adding pre-existing aerosol from the HT-22 eruption to obtain the  
273 measured AOD and using the measured SO<sub>2</sub> mass and e-folding time, results in the cyan full line in Fig. 5d.  
274 Such a combination of pre-existing aerosol from the eruption and SO<sub>2</sub> conversion is consistent with the 99.9%  
275 confidence interval of the AOD average.

276 The next question is which is the source of the pre-existing aerosol? We have no measurements of the aerosol  
277 composition to aid in this respect. From the depolarization ratio (supplementary Fig. S2) we can rule out  
278 significant fractions of volcanic ash, which is also supported by other measurements (Gupta et al., 2022; Carn et  
279 al., 2022). To find another plausible source of the pre-existing aerosol we consider the volcanological  
280 observations of hot volcanoclastic density currents entering the ocean (Seabrook et al., 2023; Clare et al., 2023)  
281 forming a boiling sea that supplies buoyancy-forming hot water vapor at the bottom of the volcanic column  
282 (Mastin et al., 2024). This process is, however, not only a source of water vapor. Gas bubbles in boiling water  
283 rise to the surface forming jet drops as well as smaller drops as the liquid film surrounding the bubble breaks at  
284 the surface. Besides liquid water these drops also contain sea salt. This results in a bimodal aerosol size  
285 distribution with large particles from the jets and small particles from the film breakage (Keene et al., 2007).  
286 High concentrations of sea salt in volcanic ash fallout from the HT-22 eruption has been documented



287 (Colombier et al., 2023). The sea salt particles from bubble bursting enter the volcanic column together with the  
288 water vapor. As the particles are hygroscopic, they readily serve as condensation nuclei in cloud formations as  
289 the air cools on the way up to the stratosphere. In the competition for water, preferentially large particles are  
290 scavenged in cloud formations prior to the formation of precipitation. This leaves the smaller particles as an  
291 interstitial aerosol (Martinsson et al., 1999). The pre-existing aerosol from the eruption (Fig. 5d) would  
292 correspond to aerosol formation from 1.1 Tg SO<sub>2</sub> based on the AOD-to-SO<sub>2</sub> ratio (Fig. 5c). Using this number as  
293 a coarse estimate on the mass of the pre-existing aerosol we can compare it with the amount of water injected  
294 into the deep BD branch (137 Tg; Fig. 2b). With the typical salinity of sea water (35 g/kg) that amount of water  
295 corresponds to 4.8 Tg of sea salt, which is four times the coarse estimate of pre-existing aerosol mass. Besides  
296 the water from bubble bursting, water evaporates directly from the heated ocean without sea salt emissions.  
297 Additional quantitative uncertainties pertain to the relative losses of water and sea salt to precipitation. Given  
298 the orders of magnitude of these estimates we can conclude that the ubiquitous aerosol formation from bubble  
299 bursting in a boiling sea is a plausible source of a pre-existing aerosol that raises global AOD to the elevated  
300 levels observed, despite the low SO<sub>2</sub> emissions.

301 Several authors have reported on the stratospheric aerosol particle size following the HT-22 eruption, i.e., 0.6 –  
302 1 μm diameter (Boichu et al., 2023), 0.8 μm (Duchamp et al., 2023) and 2 – 3 μm (Legras et al., 2022). Whereas  
303 the former two estimates show good agreement, the latter, based on estimating the gravitational settling velocity,  
304 stands out by finding the particles to be larger than the other estimates. We used the same method as Legras et  
305 al., (2022) to estimate the settling velocity:  $V(\text{sedimentation}) = V(\text{aerosol}) - V(\text{air})$ , where  $V$  is the vertical  
306 velocity,  $V(\text{aerosol})$  the observed weekly change in the aerosol centroid altitude and  $V(\text{air})$  is estimated from the  
307 weekly change in the altitude of the water vapor centroid. Applying a 3-week moving average dampened  
308 variations (Fig. 5e). The gravitational settling velocity varies around the value 20 m/day, agreeing well with the  
309 results of Legras et al. (2022) whereas the conversion to particle size differs. The settling velocity of a given  
310 particle depends on the pressure and temperature because of the air viscosity and the Cunningham slip  
311 correction factor's dependence on the mean free path of the air. We computed the particle size that best fits the  
312 weekly settling velocity observations. Fig. 5e shows decreased settling velocity as the aerosol falls to lower  
313 altitude. We found that the equivalent aerodynamic diameter was 1.1 μm, which is based on the assumptions of  
314 a spherical particle shape and particle density of 1 g/cm<sup>3</sup>. The low depolarization ratio (supplementary Fig. S2)  
315 validates the first assumption. The density of the particles is not known a priori. However, the low relative  
316 humidity (Figs. 5a and b) results in concentrated solution drops of sulfuric acid and sea salts, having density  
317 clearly exceeding 1 g/cm<sup>3</sup>, e.g., a 76.5% sulfuric acid – water solution has a density of 1.75 g/cm<sup>3</sup> at  
318 stratospheric conditions (Myhre et al., 1998). Applying that density results in 0.70 μm geometric diameter and  
319 changing the density to 1.5 and 2 g/cm<sup>3</sup> results 0.81 and 0.62 μm diameter, respectively, which is in good  
320 agreement with estimates based on other methods. Based on our results and others (Boichu et al., 2023;  
321 Duchamp et al., 2023) we conclude that the HT-22 aerosol is submicron in diameter, in between stratospheric  
322 background and Mt. Pinatubo particle sizes (Bauman et al., 2003; Wilson et al., 2008).

323 The water vapor injected into the deep BD branch remained in the stratosphere for the full two years of this  
324 study, although 23% was transported from the deep BD branch to the shallow one 1.5 years after the eruption  
325 (Fig. 2b). The stratospheric AOD remained almost constant for one year before starting to decline (Fig. 4a).



326 Because of the gravitational settling aerosol remains shorter time in the stratosphere than gases with low  
327 chemical reactivity. The combined effect of the 2019 Raikoke and Ulawun eruptions on the maximum global  
328 stratospheric AOD is the highest observed for recent eruptions (Table 1) when also the lowest part of the  
329 stratosphere are accounted for. The peak AOD from HT-22 eruption is slightly lower. However, the long  
330 duration of the AOD from the HT-22 eruption, caused by the powerful eruption placing the effluents in the deep  
331 BD branch in the tropics, makes it the most important in terms of stratospheric AOD since the 1991 eruption of  
332 Mt. Pinatubo (Fig. 5f). The first year after the eruption the AOD was 0.016. Subtracting average background  
333 AOD (Friberg et al., 2018) the stratospheric global mean AOD from the HT-22 eruption becomes 0.010. This  
334 corresponds to  $-0.24 \text{ W/m}^2$  in global stratospheric total volcanic effective radiative forcing during the first year  
335 after the eruption, according to results based on volcanic activity years 1979 to 2015 (Schmidt et al., 2018).

336 The HT-22 was the last major volcanic eruption to be studied based on data from the CALIOP lidar aboard the  
337 CALIPSO satellite that ended its mission in June 2023. This is by far the most efficient method for studies of the  
338 initial months of stratospheric aerosol formation following volcanic eruptions and wildfires, because of its  
339 brilliant vertical resolution and optically short vertical path. Limb-viewing techniques suffer from event  
340 termination (saturation) during 2 – 3 months after a major stratospheric aerosol event (Martinsson et al., 2022;  
341 Fromm et al., 2014; Chen et al., 2018; DeLand, 2019). Fig. 5f illustrates the importance of CALIOP by showing  
342 the AOD of two volcanic eruptions and one wildfire. Conversion of  $\text{SO}_2$  formed the Raikoke aerosol, resulting  
343 in 2 – 3 months delay before the AOD peaked which is the case for most volcanic eruptions (Friberg et al.,  
344 2018). In contrast, a pre-existing aerosol from HT-22 dominated its AOD and we observed the maximum  
345 already after two weeks. That was the time required for the aerosol to become dispersed enough to allow  
346 approximately ten CALIOP measurements per day in the volcanic effluents, thereby reducing the uncertainty in  
347 the daily average. Another special case was the 2017 Canadian wildfire where we observed a strong and rapid  
348 decline of the stratospheric AOD (Fig. 5f) indicative of photolytic loss of organic aerosol (Martinsson et al.,  
349 2022). A study of the 2019/2020 Australian wildfire showed similar losses, where also a complex feed of  
350 wildfire aerosol from the upper troposphere during 1 – 2 weeks after the fire was identified (Friberg et al.,  
351 2023), thanks to the mentioned special properties of the CALIOP instrument. The decommissioning of the  
352 ageing CALIOP in June 2023 severely diminishes future studies of aerosol formation and losses in the  
353 stratosphere, prompting the need for new satellite-based lidar systems.

#### 354 4 Conclusions

355 Aerosol and water vapor in the stratosphere emanating from the 15 January 2022 eruption in Hunga Tonga (HT-  
356 22) is investigated using satellite-based instruments CALIOP and MLS. Most of its effluents were injected into  
357 the deep branch of the stratospheric Brewer-Dobson (BD) circulation.

358 A small fraction of the record-breaking water vapor injections into the deep BD branch reached up to the  
359 stratopause after 1.25 years in the stratosphere, whereas 23% was transported down to the shallow BD branch as  
360 the water vapor spread vertically. The water vapor injected into the deep BD branch remained in the stratosphere  
361 for the full two years of this study. The water vapor from the HT-22 eruption in the southern tropics steadily  
362 increased its latitudinal coverage, first to the southern midlatitudes. After a year most of the global stratosphere



363 was covered with water vapor from the HT-22 eruption, before a reduction of the tropical stratospheric  
364 concentration appeared as the BD circulation brought tropospheric air that was unaffected by the HT-22  
365 eruption.

366 The aerosol and its precursor gases were initially at the same altitude as the water vapor from the HT-22  
367 eruption, but gravitational settling of the aerosol particles gradually opened a gap in altitude which resulted in  
368 the aerosol from the HT-22 eruption mainly appearing in the tropics and the southern hemisphere. The  
369 stratospheric aerosol optical depth (AOD) remained constant for a year after the eruption, before transport out of  
370 the stratosphere started. At the time of the decommission of the CALIOP instrument in June 2023, 50% of the  
371 aerosol from the HT-22 eruption had been removed from the stratosphere.

372 The AOD level of the stratosphere was established already 2 weeks after the eruption and was unexpectedly  
373 high for a modest injection of 0.4 – 0.5 Tg SO<sub>2</sub>. Given the exceptional water vapor amounts from the HT-22  
374 eruption, we investigated if hygroscopic growth affected the aerosol optical properties. Despite the record-  
375 breaking water vapor emissions, the average relative humidity remained below 5% in the dry stratosphere,  
376 causing no or limited hygroscopic growth.

377 The gravitational settling velocity of the aerosol is estimated from the altitude evolution to ~20 m/day,  
378 corresponding to an equivalent aerodynamic diameter of 1.1 μm at the altitude of the aerosol layer. Assuming  
379 density of concentrated solution drops of 1.5 – 2 g/cm<sup>3</sup> the geometrical diameter becomes 0.6 – 0.8 μm.

380 Comparing eight recent volcanic eruptions we find that the global AOD per mass of SO<sub>2</sub> emitted from the HT-22  
381 eruption is 4 times that of most other eruptions. The amount of SO<sub>2</sub> and ash emitted to the stratosphere was  
382 unusually small for an eruption with volcanic explosivity index (VEI) of 6. Widespread damage to the seafloor  
383 in runouts exceeding 100 km was caused by volcanoclastic density currents causing a boiling sea that supplied  
384 buoyancy-forming hot water vapor that amplified the eruption column. Intense aerosol formation from bubble-  
385 bursting in the boiling ocean provides sea salt aerosol being a plausible explanation for the unexpectedly high  
386 AOD.

387 The maximum global stratospheric AOD following the HT-22 eruption is among the highest observed in more  
388 than 30 years. The injection in the deep branch of DB circulation prolonged the perturbation of the stratospheric  
389 aerosol, making the HT-22 eruption the largest aerosol event since that of Mt. Pinatubo in 1991. The 1-year  
390 average global AOD of 0.01 from the HT-22 eruption can be estimated to -0.24 W/m<sup>2</sup> in global stratospheric  
391 total volcanic effective radiative forcing.

## 392 References

393 Andersson, S. M., Martinsson, B. G., Friberg, J., Brenninkmeijer, C. A. M., Rauthe-Schöch, A., Hermann,  
394 M., van Velthoven, P. F. J., and Zahn, A.: Composition and evolution of volcanic aerosol from  
395 eruptions of Kasatochi, Sarychev and Eyjafjallajökull in 2008–2010 based on CARIBIC observations,  
396 *Atmos. Chem. Phys.*, 13, 1781–1796, <https://doi.org/10.5194/acp13-1781-2013>, 2013.



- 397 Andersson, S. M., Martinsson, B. G., Vernier, J. P., Friberg, J., Brenninkmeijer, C. A. M., Hermann, M., van  
398 Velthoven, P. F. J., and Zahn, A.: Significant radiative impact of volcanic aerosol in the lowermost  
399 stratosphere, *Nat. Commun.*, 6, 1–8, <https://doi.org/10.1038/ncomms8692>, 2015.
- 400 Bauman J. J., P. B. Russell, M. A. Geller, and P. Hamill, A stratospheric aerosol climatology from SAGE II  
401 and CLAES measurements: 2. Results and comparisons, 1984–1999, *J. Geophys. Res.*, 108(D13),  
402 4383, doi:10.1029/2002JD002993, 2003.
- 403 Bernath P., C. Boone, A. Pastorek, D. Cameron and M. Lecours, Satellite characterization of global  
404 stratospheric sulfate aerosols released by Tonga volcano. *J. Quant. Spectrosc. Rad. Transf.* 299,  
405 108520, 2023.
- 406 Boichu M., R. Grandin, L. Blarel, B. Torres, Y. Derimian, P. Goloub, C. Brogniez, I. Chiapello, O. Dubovic,  
407 T. Mathurin, N. Pascal, M. Patou and J. Riedi, Growth and Global Persistence of Stratospheric Sulfate  
408 Aerosols From the 2022 Hunga Tonga–Hunga Ha'apai Volcanic Eruption. *J. Geophys. Res. Atmos.* 128,  
409 e2023JD039010. <https://doi.org/10.1029/2023JD039010>, 2023.
- 410 Bourassa, A. E., Zawada, D. J., Rieger, L. A., Warnock, T. W., Toohey, M., & Degenstein, D. A.,  
411 Tomographic retrievals of Hunga Tonga–Hunga Ha'apai volcanic aerosol. *Geophysical Research*  
412 *Letters*, 50, e2022GL101978. <https://doi.org/10.1029/2022GL101978>, 2023.
- 413 Carn S.A., N.A. Krotkov, B.L. Fisher and C. Li, Out of the blue: Volcanic SO<sub>2</sub> emissions during the 2021–  
414 2022 eruptions of Hunga Tonga—Hunga Ha'apai (Tonga). *Front. Earth Sci.* 10:976962. doi:  
415 10.3389/feart.2022.976962, 2022.
- 416 Carr J.L., A. Horváth, D.L. Wu, and M.D. Friberg, Stereo plume height and motion retrievals for the  
417 record-setting Hunga TongaHunga Ha'apai eruption of 15 January 2022. *Geophysical Research Letters*  
418 49, e2022GL098131, <https://doi.org/10.1029/2022GL098131>, 2022.
- 419 Chen, Z., Bhartia, P. K., Loughman, R., Colarco, P., and De Land, M.: Improvement of stratospheric  
420 aerosol extinction retrieval from OMPS/LP using a new aerosol model, *Atmos. Meas. Tech.*, 11, 6495–  
421 6509, <https://doi.org/10.5194/amt-11-6495-2018>, 2018.
- 422 Clare M.A., I.A. Yeo, S. Watson, R. Wysoczanski, S. Seabrook, K. Mackay, J.E. Hunt, E. Lane, P.J. Talling,  
423 E. Pope, S. Cronin, M. Ribó, T. Kula, D. Tappin, S. Henrys, C. de Ronde, M. Urlaub, S. Kutterolf, S.  
424 Fonua, S. Panuve, D. Veverka, R. Rapp, V. Kamalov and M. Williams, Fast and destructive density  
425 currents created by ocean-entering volcanic eruptions. *Science* 381, 1085–1092, 2023.
- 426 Clarisse L., D. Hurtmans, C. Clerbaux, J. Hadji-Lazaro, Y. Ngadi, and P.-F. Coheur, Retrieval of sulphur  
427 dioxide from the infrared atmospheric sounding interferometer (IASI). *Atmos. Meas. Tech.*, 5, 581–  
428 594, 2012.
- 429 Colombier M., I. A. Ukstins, S. Tegtmeier, B. Scheu, S. J. Cronin, S. Thivet, J. Paredes-Mariño, C.  
430 Cimarelli, K.-U. Hess, T. Kula, F.H. Latu'ila and D. B. Dingwell, Atmosphere injection of sea salts  
431 during large explosive submarine volcanic eruptions. *Scientific Reports* 13:14435,  
432 <https://doi.org/10.1038/s41598-023-41639-8>, 2023.
- 433 DeLand, M.: Readme document for the Soumi-NPP OPMS LP L2 AER675 Daily product, Goddard Earth  
434 Sciences Data and Information Services Center (GES DISC), <http://disc.gsfc.nasa.gov> (last access:  
435 October 2021), 2019.



- 436 Duchamp C., F. Wrana, B. Legras, P. Sellitto, R. Belhadji and C. von Savigny, Observation of the Aerosol  
437 Plume From the 2022 Hunga Tonga—Hunga Ha'apai Eruption With SAGE III/ISS. *Geophys. Res. Lett.*  
438 50, e2023GL105076, <https://doi.org/10.1029/2023GL105076>, 2023.
- 439 Friberg J., Martinsson B. G., Andersson S. M., Brenninkmeijer C. A. M., Hermann M., Van Velthoven P. F.  
440 J., and Zahn A., Sources of increase in lowermost stratospheric sulphurous and carbonaceous aerosol  
441 background concentrations during 1999–2008 derived from CARIBIC flights, *Tellus B*, 66, 23428,  
442 <https://doi.org/10.3402/tellusb.v66.23428>, 2014.
- 443 Friberg, J., Martinsson, B. G., Andersson, S. M., and Sandvik, O. S.: Volcanic impact on the climate– the  
444 stratospheric aerosol load in the period 2006–2015, *Atmos. Chem. Phys.*, 18, 11149–11169,  
445 <https://doi.org/10.5194/acp-18-11149-2018>, 2018.
- 446 Friberg J., B.G. Martinsson, and M.K. Sporre, Short- and long-term stratospheric impact of smoke from the  
447 2019–2020 Australian wildfires. *Atmos. Chem. Phys.*, 23, 12557–12570, 2023  
448 <https://doi.org/10.5194/acp-23-12557-2023>, 2023.
- 449 Fromm M., Lindsey D. T., Servranckx, R., Yue G., Trickl T., Sica R., Doucet P., and Godin-Beekmann S.,  
450 The untold story of pyrocumulonimbus, *B. Am. Meteorol. Soc.*, 91, 1193–1209, 2010.
- 451 Fromm, M., Kablick III, G., Nedoluha, G., Carboni, E., Grainger, R., Campbell, J., and Lewis, L.:  
452 Correcting the record of volcanic stratospheric aerosol impact: Nabro and Sarychev Peak, *J. Geophys.*  
453 *Res.-Atmos.*, 119, 1–22, <https://doi.org/10.1002/2014JD021507>, 2014.
- 454 Fueglistaler S., Dessler A. E., Dunkerton T. J., Folkins I., Fu Q., and Ote P. W., Tropical tropopause layer,  
455 *Rev. Geophys.*, 47, RG1004, <https://doi.org/10.1029/2008RG000267>, 2009.
- 456 Garofalo, L. A., Levin, E. J. T., Campos, T., Kreidenweis, S. N., and Farmer, D. K.: Emission and evolution  
457 of submicron organic aerosol in smoke from wildfires in the western United States, *ACS Space Chem.*,  
458 3, 1237–1247, 2019.
- 459 Gupta A.K., R. Bennartz, K.E. Fauria and T. Mittal, Eruption chronology of the December 2021 to January  
460 2022 Hunga Tonga-Hunga Ha'apai eruption sequence. *Comm. Earth Environm.* 3:314,  
461 <https://doi.org/10.1038/s43247-022-00606-3>, 2022.
- 462 Haarig, M., Ansmann, A., Baars, H., Jimenez, C., Veselovskii, I., Engelmann, R., and Althausen, D.:  
463 Depolarization and lidar ratios at 355, 532, and 1064nm and microphysical properties of aged  
464 tropospheric and stratospheric Canadian wildfire smoke, *Atmos. Chem. Phys.*, 18, 11847–11861,  
465 <https://doi.org/10.5194/acp-18-11847-2018>, 2018.
- 466 Hoffmann A., C. Ritter, M. Stock, M. Maturilli, S. Eckhardt, A. Herber, and R. Neuber, Lidar  
467 measurements of the Kasatochi aerosol plume in August and September 2008 in Ny-Ålesund,  
468 Spitsbergen. *J. Geophys. Res.*, 115, D00L12, doi:10.1029/2009JD013039, 2010.
- 469 Hu, Q., Goloub, P., Veselovskii, I., Bravo-Aranda, J.-A., Popovici, I. E., Podvin, T., Haeffelin, M., Lopatin,  
470 A., Dubovik, O., Pietras, C., Huang, X., Torres, B., and Chen, C.: Long-range transported Canadian  
471 smoke plumes in the lower stratosphere over northern France, *Atmos. Chem. Phys.*, 19, 1173–1193,  
472 <https://doi.org/10.5194/acp-19-1173-2019>, 2019.
- 473 Kahn, R. A., Limbacher, J. A., Junghenn Noyes, K. T., Flower, V. J. B., Zamora, L. M., & McKee, K. F.,  
474 Evolving particles in the 2022 Hunga Tonga— Hunga Ha'apai volcano eruption plume. *J. Geophys.*  
475 *Res.*, 129, e2023JD039963. <https://doi.org/10.1029/2023JD039963>, 2024.



- 476 Keene W.C., H. Maring, J.R. Maben, D.J. Kieber, A.A.P. Pszenny, E.E. Dahl, M.A. Izaguirre, A.J. Davis,  
477 M.S. Long, X. Zhou, L. Smoydzin, and R. Sander, Chemical and physical characteristics of nascent  
478 aerosols produced by bursting bubbles at a model air-sea interface, *J. Geophys. Res.*, 112, D21202,  
479 doi:10.1029/2007JD008464, 2007.
- 480 Khaykin S., A. Podglajen, F. Ploeger, J.-U. Grooß, F. Tence, S. Bekki, K. Khlopenkov, K. Bedka, L.  
481 Rieger, A. Baron, S. Godin-Beekmann, B. Legras, P. Sellitto, T. Sakai, J. Barnes, O. Uchino, I. Morino,  
482 T. Nagai, R. Wing, G. Baumgarten, M. Gerding, V. Duflot, G. Payen, J. Jumelet, R. Querel, B. Liley, A.  
483 Bourassa, B. Clouser, A. Feofilov, A. Hauchecorne and F. Ravetta, Global perturbation of stratospheric  
484 water and aerosol burden by Hunga eruption. *Comm. Earth Environm.*, 3:316,  
485 <https://doi.org/10.1038/s43247-022-00652-x>|[www.nature.com/commsenv](http://www.nature.com/commsenv), 2022.
- 486 Klekociuk A.R., D.J. Ottaway, A.D. MacKinnon, I.M. Reid, L.M. Twigger and S.P. Alexander, Australian  
487 Lidar Measurements of Aerosol Layers Associated with the 2015 Calbuco Eruption. *Atmosphere* 11,  
488 124, 2020.
- 489 Kloss C., G. Berthet, P. Sellitto, F. Ploeger, G. Taha, M. Tidiga, M. Eremenko, A. Bossolasco, F. Jégou, J.-  
490 B. Renard, and B. Legras, Stratospheric aerosol layer perturbation caused by the 2019 Raikoke and  
491 Ulawun eruptions and their radiative forcing. *Atmos. Chem. Phys.*, 21, 535–560, 2021.
- 492 Kremser, S., Thomason, L. W., von Hobe, M., Hermann, M., Desher, T., Timmreck, C., Toohey, M.,  
493 Stenke, A., Schwarz, J. P., Weigel, R., Fueglistaler, S., Prata, F. J., Vernier, J. P., Schlager, H., Barnes, J.  
494 E., Antuña-Marrero, J. C., Fairlie, D., Palm, M., Mahieu, E., Notholt, J., Rex, M., Bingen, C.,  
495 Vanhellefont, F., Bourassa, A., Plane, J. M. C., Klocke, D., Carn, S. A., Clarisse, L., Trickl, T., Neely,  
496 R., James, A. D., Rieger, L., Wilson, J. C., and Meland, B.: Stratospheric aerosol– Observations,  
497 processes, and impact on climate, *Rev. Geophys.*, 54, 278–335,  
498 <https://doi.org/10.1002/2015RG000511>, 2016.
- 499 Lambert, A., Read, W., and Livesey, N.: MLS/Aura Level 2 Water Vapor (H<sub>2</sub>O) Mixing Ratio V005,  
500 Greenbelt, MD, USA, Goddard Earth Sciences Data and Information Services Center (GES DISC),  
501 <https://doi.org/10.5067/Aura/MLS/DATA2508>, 2020.
- 502 Legras B., C. Duchamp, P. Sellitto, A. Podglajen, E. Carboni, R. Siddans, J.-U. Grooß, S. Khaykin, and F.  
503 Ploeger, The evolution and dynamics of the Hunga Tonga–Hunga Ha’apai sulfate aerosol plume in the  
504 stratosphere. *Atmos. Chem. Phys.*, 22, 14957–14970, 2022.
- 505 Li C., N.A. Krotkov, S. Carn, Y. Zhang, R.J.D. Spurr, and J. Joiner, New-generation NASA Aura Ozone  
506 Monitoring Instrument (OMI) volcanic SO<sub>2</sub> dataset: algorithm description, initial results, and  
507 continuation with the Suomi-NPP Ozone Mapping and Profiler Suite (OMPS). *Atmos. Meas. Tech.*, 10,  
508 445–458, 2017.
- 509 Livesey, N. J., Read, W. G., Wagner, P. A., Froidevaux, L., Santee, M. L., Schwartz, M. J., Lambert, A.,  
510 Manney, G. L., Valle, L. F. M., Pumphrey, H. C., Fuller, R. A., Jarnot, R. F., Knosp, B. W., and Lay,  
511 R.R.: EOS MLS Version 5.0x Level2 and 3 data quality and description document, Tech. rep., Jet  
512 Propulsion Laboratory D734 105336 Rev. A, <https://mls.jpl.nasa.gov/publications>, 2020.
- 513 Martinsson B.G., G. Frank, S.-I. Cederfelt, E. Swietlicki, O.H. Berg, J. Zhou, K.N. Bower, C. Bradbury, W.  
514 Birmili, F. Stratmann, M. Wendisch, A. Wiedensohler, B.A. Yuskiewicz, Droplet nucleation and growth  
515 in orographic clouds in relation to the aerosol population. *Atmos. Res.* 50, 289–315, 1999.



- 516 Martinsson, B. G., Brenninkmeijer, C. A. M., Cam, S. A., Hermann, M., Heue, K.P., van Velthoven, P. F. J.,  
517 and Zahn, A.: Influence of the 2008 Kasatochi volcanic eruption on sulfurous and carbonaceous  
518 aerosol constituents in the lower stratosphere, *Geophys. Res. Lett.*, 36, 1–5,  
519 <https://doi.org/10.1029/2009GL038735>, 2009.
- 520 Martinsson, B. G., Friberg, J., Sandvik, O. S., Hermann, M., van Velthoven, P. F. J., and Zahn, A.:  
521 Formation and composition of the UTLS aerosol, *Npj Climate and Atmospheric Science*, 2, 1–6,  
522 <https://doi.org/10.1038/s41612-019-0097-1>, 2019.
- 523 Martinsson, B. G., Friberg, J., Sandvik, O. S., and Sporre, M. K.: Five-satellite-sensor study of the rapid  
524 decline of wildfire smoke in the stratosphere, *Atmos. Chem. Phys.*, 22, 3967–3984,  
525 <https://doi.org/10.5194/acp-22-3967-2022>, 2022.
- 526 Mastin L.G., A.R. Van Eaton and S.J. Cronin, Did steam boost the height and growth rate of the giant  
527 Hunga eruption plume? *Bull. Volcanology* 86:64, <https://doi.org/10.1007/s00445-024-01749-1>, 2024.
- 528 Millán, L., Santee, M. L., Lambert, A., Livesey, N. J., Werner, F., Schwartz, M. J., Pumphrey H.C., Manney  
529 G.L., Wang Y., Su H., Read W.G. and Froidevaux H.C., The Hunga Tonga-Hunga Ha'apai Hydration of  
530 the Stratosphere. *Geophysical Research Letters*, 49, e2022GL099381. <https://doi.org/10.1029/2022GL099381>, 2022.
- 531
- 532 Murphy, D. M. and Koop, T., Review of the vapour pressures of ice and supercooled water for atmospheric  
533 applications, *Q. J. Roy. Meteor. Soc.*, 131, 1539–1565, <https://doi.org/10.1256/qj.04.94>, 2005.
- 534 Murphy D. M., Cziczo D. J., Hudson P. K., and Thomson D. S., Carbonaceous material in aerosol particles  
535 in the lower stratosphere and tropopause region, *J. Geophys. Res.*, 112, D04203,  
536 <https://doi.org/10.1029/2006JD007297>, 2007.
- 537 Myhre C.E.L., C.J. Nielsen, and O.W. Saastad, Density and Surface Tension of Aqueous H<sub>2</sub>SO<sub>4</sub> at Low  
538 Temperature. *J. Chem. Eng. Data* 43, 617–622, 1998.
- 539 Nedoluha G.E., Gomez R.M., Boyd I., Neal H., Allen D.R. and Lambert A., The spread of the Hunga Tonga  
540 H<sub>2</sub>O plume in the middle atmosphere over the first two years since eruption. *J. Geophys. Res. Atmos.*  
541 129, e2024JD040907. <https://doi.org/10.1029/2024JD040907>, 2024.
- 542 O'Neill N.T., C. Perro, A. Saha, G. Lesins, T. J. Duck, E. W. Eloranta, G. J. Nott, A. Hoffman, M. L.  
543 Karumudi, C. Ritter, A. Bourassa, I. Abboud, S. A. Carn, and V. Savastiouk, Properties of Sarychev  
544 sulphate aerosols over the Arctic, *J. Geophys. Res.*, 117, D04203, doi:10.1029/2011JD016838, 2012.
- 545 Pardini F., M. Burton, F. Arzilli, G. La Spina, M. Polacci, SO<sub>2</sub> emissions, plume heights and magmatic  
546 processes inferred from satellite data: The 2015 Calbuco eruptions. *J. Volcanol. Geotherm. Res.* 361,  
547 12–24, 2018.
- 548 Poli P. and N.M. Shapiro, Rapid characterization of large volcanic eruptions: measuring the impulse of the  
549 Hunga Tonga Ha'apai explosion from teleseismic waves. *Geophys. Res. Letters* 49, e2022GL098123.  
550 <https://doi.org/10.1029/2022GL098123>, 2022.
- 551 Proud S.R., A.T. Prata and S. Schmauss, The January 2022 eruption of Hunga Tonga-Hunga Ha'apai  
552 volcano reached the mesosphere. *Science* 378, 554–557, 2022.
- 553 Sandvik O.S., J. Friberg, M.K. Sporre, and B.G. Martinsson, Methodology to obtain highly resolved SO<sub>2</sub>  
554 vertical profiles for representation of volcanic emissions in climate models. *Atmos. Meas. Tech.*, 14,  
555 7153–7165, 2021.



- 556 Schmidt, A., Mills M. J., Ghan S., Gregory J. M., Allan R. P., Andrews T., Bardeen C.G., Conley A., Forster  
557 P.M., Gettelman A., Portmann R.W., Solomon S. And Toon O.B., Volcanic radiative forcing from 1979  
558 to 2015. *J. Geophys. Res. Atmos.* 123, 12,491–12,508. <https://doi.org/10.1029/2018JD028776>, 2018.
- 559 Schoeberl, M. R., Wang, Y., Ueyama, R., Taha, G., Jensen, E., and Yu, W., Analysis and impact of the  
560 Hunga Tonga-Hunga Ha'apai stratospheric water vapor plume. *Geophysical Research Letters*, 49,  
561 e2022GL100248. <https://doi.org/10.1029/2022GL100248>, 2022.
- 562 Seabrook S., K. Mackay, S.J. Watson, M.A. Clare, J.E. Hunt, I.A. Yeo, E.M. Lane, M.R. Clark, R.  
563 Wysoczanski, A.A. Rowden, T. Kula, L.J. Hoffmann, E. Armstrong and M.J.M. Williams,  
564 Volcaniclastic density currents explain widespread and diverse seafloor impacts of the 2022 Hunga  
565 Volcano eruption. *Nat. Commun.*, 14:7881, <https://doi.org/10.1038/s41467-023-43607-2>, 2023.
- 566 Sellitto P., A. Podglajen, R. Belhadj, M. Boichu, E. Carboni, J. Cuesta, C. Duchamp, C. Kloss, R. Siddans,  
567 N. Bègue, L. Blarel, F. Jegou, S. Khaykin, J.-B. Renard and B. Legras, The unexpected radiative  
568 impact of the Hunga Tonga eruption of 15th January 2022. *Comm. Earth Environm.* 3:288  
569 [\[https://doi.org/10.1038/s43247-022-00618-z](https://doi.org/10.1038/s43247-022-00618-z), 2022.
- 570 Sellitto P., R. Siddans, R. Belhadj, E. Carboni, B. Legras, A. Podglajen, C. Duchamp, and B. Kerridge,  
571 Observing the SO<sub>2</sub> and Sulfate Aerosol Plumes From the 2022 Hunga Eruption With the Infrared  
572 Atmospheric Sounding Interferometer (IASI). *Geophys. Res. Lett.* 51, e2023GL105565.  
573 <https://doi.org/10.1029/2023GL105565>, 2024.
- 574 Taha, G., OMPS-NPP L2 LP Aerosol Extinction Vertical Profile swath daily 3slit V2, Greenbelt, MD,  
575 USA, Goddard Earth Sciences Data and Information Services Center (GES DISC),  
576 <https://doi.org/10.5067/CX2B9NW6FI27>, 2020.
- 577 Taha, G., Loughman, R., Colarco, P. R., Zhu, T., Thomason, L. W., and Jaross, G., Tracking the 2022  
578 Hunga Tonga-Hunga Ha'apai aerosol cloud in the upper and middle stratosphere using space-based  
579 observations. *Geophysical Research Letters*, 49, e2022GL100091.  
580 <https://doi.org/10.1029/2022GL100091>, 2022.
- 581 Taylor I.A., R.G. Grainger, A.T. Prata, S.R. Proud, T.A. Mather, and D.M. Pyle, Asatellite chronology of  
582 plumes from the April 2021 eruption of La Soufrière, St Vincent. *Atmos. Chem. Phys.*, 23, 15209–  
583 15234, 2023.
- 584 Vernier J.-P., Thomason L. W., Pommereau J. P., Bourassa A., Pelon J., Garnier A., Hauchecorne A., Blanot  
585 L., Trepte C., Degenstein D., and Vargas F., Major influence of tropical volcanic eruptions on the  
586 stratospheric aerosol layer during the last decade, *Geophys. Res. Lett.*, 38, 1–8,  
587 <https://doi.org/10.1029/2011GL047563>, 2011.
- 588 Vernier J.-P., D. Farlie, T. Deshler, M. Natarajan, T. Knepp, K. Foster, F.G. Weingold, K.M. Bedka, L.  
589 Thomason and C. Trepte, In situ and space-based observations of the Kelud volcanic plume: The  
590 persistence of ash in the lower stratosphere. *J. Geophys. Res. Atmos.* 121, 11,104–11,118, doi:10.1002/  
591 2016JD025344, 2016.
- 592 Voudouri K.A., K. Michailidis, M.-E. Koukoulis, S. Rémy, A. Inness, G. Taha, G. Peletidou, N. Siomos, D.  
593 Balis and M. Parrington, Investigating a Persistent Stratospheric Aerosol Layer Observed over  
594 Southern Europe during 2019. *Remote Sens.* 15, 5394. <https://doi.org/10.3390/rs15225394>, 2023.



- 595 Waters, J. W., Froidevaux, L., Harwood, R., Jarnot, R., Pickett, H., Read, W., Siegel, P., Cofield, R.,  
596 Filipiak, M., Flower, D., Holden, J., Lau, G., Livesey, N., Manney, G., Pumphrey, H., Santee, M., Wu,  
597 D., Cuddy, D., Lay, R., Loo, M., Perun, V., Schwartz, M., Stek, P., Thurstans, R., Boyles, M., Chandra,  
598 S., Chavez, M., Chen, G.-S., Chudasama, B., Dodge, R., Fuller, R., Girard, M., Jiang, J., Jiang, Y.,  
599 Knosp, B., LaBelle, R., Lam, J., Lee, K., Miller, D., Oswald, J., Patel, N., Pukala, D., Quintero, O.,  
600 Scaff, D., Snyder, W., Tope, M., Wagner, P., and Walch, M.: The earth observing system microwave  
601 limb sounder (EOS MLS) on the Aura satellite, *IEEE T. Geosci. Remote*, 44, 1106–1121, 2006
- 602 Wilson J.C., S.-H. Lee, J. M. Reeves, C. A. Brock, H. H. Jonsson, B. G. Lafleur, M. Loewenstein, J.  
603 Podolske, E. Atlas, K. Boering, G. Toon, D. Fahey, T. P. Bui, G. Diskin, and F. Moore, Steady-state  
604 aerosol distributions in the extra-tropical, lower stratosphere and the processes that maintain them.  
605 *Atmos. Chem. Phys.*, 8, 6617–6626, 2008.
- 606 Winker, D. M., Hunt, W. H., and McGill, M. J.: Initial performance assessment of CALIOP, *Geophys. Res.*  
607 *Letts.*, 34, 1–5, <https://doi.org/10.1029/2007GL030135>, 2007.
- 608 Winker, D. M., Pelon, J., Coakley, J. A., Ackerman, S. A., Charlson, R. J., Colarco, P. R., Flamant, P., Fu,  
609 Q., Hoff, R. M., Kittaka, C., Kubar, T. L., Le Treut, H., McCormick, M. P., Mégie, G., Poole, L.,  
610 Powell, K., Trepte, K., Vaughan, M. A., and Wielicki, B. A.: The CALIPSO mission— A global 3D view  
611 of aerosols and clouds, *B. Am. Meteorol. Soc.*, 91, 1211–1229,  
612 <https://doi.org/10.1175/2010BAMS3009.1>, 2010.
- 613 Winkler P., The growth of atmospheric aerosol particles as a function of the relative humidity – II Improved  
614 concept of mixed nuclei. *Aerosol Sci.* 4, 373-387, 1973.
- 615 Xu J., D. Li D., Z. Bai, M. Tao and J. Bian, Large Amounts of Water Vapor Were Injected into the  
616 Stratosphere by the Hunga Tonga–Hunga Ha’apai Volcano Eruption. *Atmosphere* 13, 912. <https://doi.org/10.3390/atmos13060912>, 2022.
- 618 Yang, K., X. Liu, P. K. Bhartia, N. A. Krotkov, S. A. Carn, E. J. Hughes, A. J. Krueger, R. J. D. Spurr, and  
619 S. G. Trahan, Direct retrieval of sulfur dioxide amount and altitude from spaceborne hyperspectral UV  
620 measurements: Theory and application. *J. Geophys. Res.*, 115, D00L09, doi:10.1029/2010JD013982,  
621 2010.
- 622 Zhu Y., C.G. Bardeen, S. Tilmes, M.J. Mills, X. Wang, V. Lynn Harvey G. Taha, D. Kinnison, R.W.  
623 Portmann, P. Yu, K.H. Rosenlof, M. Avery, C. Kloss, C. Li, A.S. Glanville, L. Millán, T. Deshler, N.  
624 Krotkov and O.B. Toon, Perturbations in stratospheric aerosol evolution due to the water-rich plume of  
625 the 2022 Hunga-Tonga eruption. *Comm. Earth Environm.* 3:248, [https://doi.org/10.1038/s43247-022-](https://doi.org/10.1038/s43247-022-00580-w)  
626 00580-w, 2022.
- 627 Zhuang J. and F. Yi, Nabro aerosol evolution observed jointly by lidars at a mid-latitude site and CALIPSO.  
628 *Atmos. Environm.* 140, 106-116, 2016.
- 629 *Data availability.* The data used are publicly available: CALIOP V4.51 lidar data (<https://search.earthdata.nasa.gov/search?fp=CALIPSO>), and MLS data (version 5.0-1.0a, level 2) from [https://disc.gsfc.nasa.gov/datasets?page=1&keywords=ML2H2O\\_005](https://disc.gsfc.nasa.gov/datasets?page=1&keywords=ML2H2O_005).
- 632 *Author contributions.* BGM planned the study, undertook most of the data analysis and wrote the paper. JF  
633 undertook part of the data analysis and MKS contributed. JF and MKS undertook data extraction and handling  
634 for the data analysis. All authors participated in discussions and commented on the manuscript.



635 *Disclaimer.* The contact author and the co-authors declare that they have no competing interests.

636 *Acknowledgements.* Aerosol products from the CALIOP sensor were produced by NASA Langley Research  
637 Center. Water vapor and temperature profiles from MLS are supplied by Goddard Earth Sciences Data and  
638 Information Services Center.

639 *Financial support.* The Swedish National Space Agency, contract 2022-00157, Johan Friberg. The Crafoord  
640 Foundation, contract 20240901, Johan Friberg. Formas, contract 2020-00997, Moa Sporre. The Swedish  
641 Research Council 2022-02836, Moa Sporre.